Characterising the chemistry of micropores in a sodic soil with strong texture-contrast using synchrotron X-ray techniques and LA-ICP-MS

Laurence Jassogne, Ganga Hettiarachchi, Ann McNeill, David Chittleborough

Published Version Information

Citation: Jassogne, L., Hettiarachchi, G., McNeill, A., & Chittleborough, D. (2012). Characterising the chemistry of micropores in a sodic soil with strong texture-contrast using synchrotron X-ray techniques and LA-ICP-MS. Soil Research, 50(5), 424-435.

Digital Object Identifier (DOI): doi:10.1071/SR11312

Publisher's Link: http://www.publish.csiro.au/?paper=SR11312

Characterising the chemistry of micropores in a sodic soil with strong texture-contrast using synchrotron X-ray techniques and LA-ICP-MS

Laurence Jassogne[1], Ganga Hettiarachchi*[2,3], Ann McNeill[3], David Chittleborough[4]

[1]School of Plant Biology, University of Western Australia, Crawley Western Australia, 6907

[2]Department of Agronomy, Kansas State University, Manhattan, KS 66506, USA

[3]School of Agriculture, Food and Wine, University of Adelaide, Waite Campus, PMB 1, Glen Osmond, SA, 5064 Australia.

[3]School of Earth and Environmental Sciences, University of Adelaide, Waite Campus, PMB 1, Glen Osmond, SA, 5064 Australia

*corresponding author; e-mail: ganga@ksu.edu

Phone: 785-532-7209

Fax: 785-532-6094

Acknowledgments:

We thank the Australian government for the International Postgraduate Research Scholarship of Laurence Jassogne. We would also like to thank Prof. Hans Lambers for support. This work was performed at GeoSoilEnviroCARS (Sector 13), Advanced Photon Source (APS), Argonne National Laboratory. GeoSoilEnviroCARS is supported by the National Science Foundation - Earth Sciences (EAR-0622171) and Department of Energy - Geosciences (DE-FG02-94ER14466). Use of the Advanced Photon Source was supported by the U. S. Department of Energy, Office of Science, Office of Basic Energy Sciences, under Contract No. DE-AC02-06CH11357. We especially want to thank Matt Newville at GSECARS for the invaluable suggestions

for sample setup and support for XRF/XAS data collection. The authors would also like to thank Angus Netting for the help with LA-ICP-MS analysis at Adelaide Microscopy. This work was supported by an AINSE grant (No. 06/030P) and by the Australian Synchrotron Research Program (ASRP) which is funded by the Commonwealth of Australia under Major National Research Facilities Program. The Cooperative Research Centre for Plant-based Management of Dryland Salinity also partly funded this research.

ABSTRACT

Soils with strong texture contrast between A and B horizons dominate the agricultural zones of western and southern Australia. The B horizon is often sodic, of much finer texture than the A (or E) horizon above and can have a bulk density as high as 2 $g.cm^{-3}$. When dry, these B horizons may severely impede the root growth of annual cereal crops. The objective of this study was to characterise the mineralogy and chemistry of fine pores at the interface of an E and sodic B horizon of an Alfisol (Sodosol). Micro-X-ray fluorescence spectroscopy (μ-XRF) was used to locate the distribution of calcium (Ca), manganese (Mn), iron (Fe), zinc (Zn) and copper (Cu), and μ-X-ray absorption near edge structure (μ-XANES) spectroscopy to investigate speciation of Fe, Mn, Zn and Cu around a pore. Both natural aggregates and thin sections were employed but measurements from thin sections were more useful because of the smaller thickness of the sample. The distribution maps showed that Ca was present in the pores but not the other elements. Copper, Mn and Zn were concentrated around the micropore. Manganese was always well correlated with Fe.

Manganese was found in reduced form (i.e., Mn (II)) and associated with phosphates whereas Fe was in oxidised form and mostly associated with oxides. Zinc was mostly associated with carbonates (CO_3), sulfates (SO_4) and silicates (SiO_4). The results were then compared with measurements by Laser Ablation Inductively Coupled Plasma Mass Spectrometry (LA-ICP-MS). Only some observations made by μ-XRF were confirmed by LA-ICP-MS, most probably because of the superior detection limits of synchrotron based μ-XRF.

INTRODUCTION

Soils with strong texture contrast between surface and B horizons, called duplex soils in Australia, dominate the agricultural zones of western and southern Australia. The A and E horizons of such soils are usually coarse-textured and of low nutrient content and water holding capacity. The B horizon has a much finer texture than the surface horizons and can have a bulk density as high as 2 g cm^{-3} (Chittleborough 1992). High soil strength causes mechanical resistance to root penetration. Furthermore, root growth can be impeded because of seasonal waterlogging caused by a perched watertable on the dense, high-strength sodic B horizon (Adcock *et al*. 2007). Roots growing through the B-horizon of texture-contrast soils can use pores that extend many meters through the profile (Yunusa *et al*. 2002). These biopores, presumably created by native perennial vegetation, not only provide pathways through the soil otherwise impenetrable by many plants, but also improve exposure to preferential flows of oxygen, water and nutrients (Bouma 1992; Eldridge and Freudenberger 2005).

Roots change the chemical, physical and biological properties of the soil in which they grow and the zone of soil in which these changes occur is called the rhizosphere (Hinsinger *et al*. 2006). These effects can be direct, such as the exudation of protons which lower soil pH thereby facilitating access to nutrients, or indirect, such as the exudation of organic molecules that can be used as substrate by soil microbes. In a root system, fine roots (< 0.8 mm) and root hairs are responsible for water and nutrient uptake (McCully 1999). These roots will be located in the meso- and micropores of a structured soil. Micropores, also called matrix pores, occur between

individual mineral grains and soil particles and are not generally created by soil biota (Eldridge and Freudenberger 2005).

The rhizosphere develops, matures and senesces in parallel with developmental changes in adjacent regions of the subtending root and remains as a relic after root death, often as a biopore which, in hard soils, is occupied by roots of subsequent crops (McCully 2005). Stewart *et al*. (1999) defined the macropore sheath as the zone around a macropore in which 80 % of the roots in the soil are located. In "hostile" soils, the macropore sheath is small and the roots are concentrated in the immediate vicinity of the macropore. "Hostile" is a descriptor that has been used to convey the difficulty of many introduced crop and pasture plants to cope with duplex soils having high strength B horizons. In less hostile soils, the influence of the macropore sheath extends further into the soil matrix and roots are more evenly distributed in the soil. Few studies have looked at the chemistry of remnant rhizospheres in soil. Most studies have been carried out at the scale of millimeters and on soils in which the natural structure has been destroyed. In the study by Stewart *et al.* (1999) a 3 mm annulus around the macropore was scraped and separated from the matrix and analysed for several elements and microbiological activity. Studies on duplex soils have shown that the environment around such a macropore has higher organic C, total N, bicarbonate-extractable P, Ca, Cu, Fe and Mn, and supported higher populations of bacteria, fungi and actinomycetes (i.e. *Pseudomonas* spp., *Bacillus* spp., cellulolytic bacteria, cellulolytic fungi, nitrifying bacteria and the root pathogen *Pythium*) than the bulk soil (Pierret *et al*. 1999; Pankhurst *et al*. 2002).

Because root growth in hostile subsoils is dependent on pore character, there is a need to understand the distribution of nutrients in relation to pore surfaces. The distribution of micronutrients, the highly heterogeneous nature of soils and especially

their pore surfaces, require techniques capable of high resolution and high surface sensitivity. In a previous study Jassogne *et al*. (2009) employed synchrotron based X-ray techniques to produce high resolution maps of the distribution of Ca, Mn, Fe, Zn and Cu. Synchrotron radiation allowed differentiation of these elements with greater certainty than normal X-ray techniques of lower resolution. Our previous study (Jassogne *et al*. 2009) showed no detectable difference in speciation of these elements at the pore surface and <500 μm from it. We concluded although the influence of the micropore was to concentrate macro- and/or micronutrients within and/or in the immediate vicinity, there was no significant influence of the micropore on the chemical form of these elements. We also concluded that a larger area around the micropore should be studied to investigate whether the influence on the chemical form of these elements varies with scale.

There is a paucity of information at the nano- and micro-scale of the effect of roots on the chemistry of the pore surface and to what extent synchrotron based X-ray fluorescence (μ-XRF) and X-ray absorption near edge spectroscopy (XANES) can aid in these investigations. The X-ray beam can be focused to a spot size of amplitude of a couple of μm to 25-50 μm, depending on the beamline, using a combined harmonic rejection/vertical mirror. A study by Voegelin *et al*. (2007) used these techniques to investigate the distribution and speciation of arsenic (As) around roots in thin sections of riparian soils. The analysis of soil thin sections by μ-XRF and XANES has also been employed to investigate the speciation of Zn in clay soils (Isaure *et al*. 2005; Manceau *et al*. 2004) and the geochemistry of As, Se and Fe in soil developed in pyritic shale materials (Strawn *et al*. 2002). The benefit of using thin sections is that the surface is smooth and flat. Thin sections are also easier to handle than intact

samples. Nevertheless, impregnating a soil sample with a resin is invasive and the chemistry and structure of the sample could be altered. Drying the sample too quickly with acetone can make roots shrink and can give a misrepresentation of the soil/root contact. However, thin sections can be prepared in such a manner that the interface between soil and root is only minimally perturbed (Vannoordwijk *et al*. 1992).

In this study we analyse aggregates of soil in which the original structure has been maintained and thin sections of undisturbed soil at micrometer-scale in order to resolve the distribution of Ca, Fe, Mn, Zn and Cu around micropores by μ-XRF and their speciation by XANES. The locus of our study was the E horizon-B horizon boundary, the site in the profile of abrupt texture contrast. Because of the novelty of this study, it was important to investigate other techniques that could confirm our findings. In a previous study by Jassogne *et al*. (2009) some observations by X-ray absorption spectroscopy were confirmed by scanning electron microscopy fitted with an energy-dispersive X-ray analyser (SEM-EDXA), but the instrument was not sensitive enough to study all the elements of interest. Because LA-ICP-MS can provide spatially-resolved information at ppm detection limits for many elements (Jimenez *et al*. 2007) this technique was employed. In this paper, LA-ICP-MS was used to determine the distribution of Ca, Mn, Fe, Zn and Cu along a transect crossing a micropore.

MATERIALS AND METHODS

Intact soil cores (50 cm long, 15 cm diameter) were taken from an agricultural site in southern Australia (33° 54'S, 137° 47'E). The soil was a Red Sodosol in the Australian Soil Classification (Isbell 1996) or a Typic Natrixeralf (Soil Survey Staff

1999). It consisted of A and E horizons of sand texture overlying a sodic B horizon of clay texture at approximately 35 cm. The general characteristics of this soil are presented in another paper (Jassogne *et al*. 2009). Intact soil segments (10 cm × 10 cm × 10 cm) were excised from the zone around the E-B boundary (hereafter called the interface). These segments were impregnated with an epoxy resin and sections of thickness 20 μm prepared. Soil clods (approx. 1.5 cm × 1.5 cm × 0.7 cm) were isolated from the interface. A criterion for selection of the clods for analysis was that they had distinguishable root channels on their outer surfaces. Micropores were selected on two of the clods. The channels selected for analysis in thin sections were those containing either a decaying root or organic coatings on their surfaces (Figure 1). In two small pores at the top of the B horizon it was possible to excise with a fine needle and scalpel a sufficient and coherent amount of organic material for radiocarbon analysis at the Australian Nuclear Science and Technology Facility near Sydney by accelerator mass spectrometry. Ages were 250 and 450 years BP.

The distribution of Fe, Mn, Cu, Zn and Ca around the selected pores were mapped by μ–XRF, the speciation of Mn, Fe and Zn by μ-XANES and that of Cu by μ-X-ray absorption fine structure spectroscopy (μ-XAFS). The μ–XRF, μ–XANES and μ–XAFS data were collected at beamline 13-BM-GSECARS (GeoSoilEnviroConsortium of Advanced Radiation Sources) at the Advanced Photon Source (APS) at Argonne National Laboratory, Argonne, IL. The electron storage ring operated at 7 GeV with a top-up fill status. This bending magnet beamline is specialised for earth and environmental science research. The μ–XRF maps and μ–XANES spectra were collected at ambient temperature in fluorescence mode except for the μ–XANES spectra of the standards that were collected in transmission mode. The μ–XRF microprobe at APS beamline 13-BM is capable of collecting

fluorescence data with a 10-30 μm beam spot size range and 10 to 50 mg kg^{-1} sensitivity, thereby allowing the study of elements at low concentration in complex soil samples.

The XRF maps were taken at two energies. The high energy map was taken at 10500 keV and showed the distribution of Fe, Zn and Cu. The low energy map was taken at energy of 7050 eV. This is below the absorption edge of Fe to avoid interference from background Fe fluorescence for elements (in our study, Mn) with an absorption edge less than that of Fe and located close to the Fe absorption edge.

The intact samples and the thin sections were mounted on the rotation axis of an x-y-θ stepping motor stage. Fluorescence data were collected for a 10,000 μm by 200 μm area on the first intact sample, a 10,000 μm by 950 μm area on the second intact sample and two 2,400 μm by 1000 μm areas on the thin section. The step size was 50 μm for the intact sample and 25 μm for the thin sections using a solid-state energy dispersive X-ray detector that allowed simultaneous detection of fluorescence signals from multiple elements. Aluminium foil was used to diminish the background fluorescence from Fe. The fluorescence signal from a given element is proportional to the integrated number of atoms of that element along thetransect of the synchrotron beam.

'Hotspots'(zones of relatively high concentration) of the elements of interest were chosen based on the XRF maps. Selecting these points allowed collection of XAFS spectra, especially for elements present in very low concentrations. Hotspots were randomly selected for each element (Mn, Fe, Cu and Zn), some close to the pore surface, some further into the soil matrix. A similar procedure was adopted for the thin section analysis. Three μ–XANES spectra were collected over the energy range of -200 to + 600 eV above the K-edge. The XANES and EXAFS spectra were

collected around the absorption edges of the elements of interest: Mn; 6539 eV, Fe: 7112 eV, Cu: 8979 eV and Zn: 9659 eV. Additionally, the XANES and EXAFS spectra of Fe, Mn, Cu and Zn standards were collected. Standards were chosen carefully according to the knowledge of the type of soil. For example, the soil had a strong red colour which indicated that it potentially contained much oxidised Fe. The standards selected for Fe were fayalite (Fe_2SiO_4), magnetite (Fe_3O_4), goethite (FeOOH), siderite ($FeCO_3$), vivianite ($Fe_3(PO_4).8H_2O$), hematite (Fe_2O_3), greenrust-Cl (($Fe, Mg^{2+})_6(Fe^{3+})_2(OH)_{18}.4(H_2O)_{18}Cl$), greenrust-(($Fe,Mg^{2+})_6(Fe^{3+})_2(OH)_{18}.4(H_2O)_{18}SO_4$).. The standards selected for Mn were birnessite ($(Na,Ca)_{0.5}(Mn^{4+},Mn^{3+})_2O_4 \cdot 1.5H_2O$), hureaulite ($(Mn, Fe)_5H_2(PO_4)_4.4H_2O$), manganocalcite (Mn-$CaCO_3$), Mn-carbonate ($MnCO_3$), Mn-sulfate ($MnSO_4$), bixbyite ($Mn_2O_3$), pyrolusite ($MnO_2$) and switzrite ($(Mn, Fe)_3(PO_4)_2.7H_2O$). The standards selected for Cu were azurite ($Cu_3(CO_3)_2(OH)_2$), calcosiderite ($Cu,Fe_6(PO_4)_4(OH)_8 \cdot 4(H_2O)$), cuprite ($Cu_2O$), libethenite ($Cu_2(PO_4)(OH)$), malachite ($Cu_2(CO_3)(OH)_2$), nissonite ($Cu_2Mg_2(PO_4)_2(OH)_2 \cdot 5(H_2O)$), pseudomalachite ($Cu_5(PO_4)_2(OH)_4$), tenorite (CuO) and $CuSO_4$. The standards selected for Zn were ferrihydrite adsorbed Zn (Zn-$Fe_5O_3(OH)_9$), franklenite ($Zn,Mn^{2+},Fe^{2+})(Fe^{3+},Mn^{3+})_2O_4$), hopeite ($Zn_3(PO_4)_2 \cdot 4(H_2O)$), hydrozincite (($Zn_5(CO_3)_2(OH)_6$), scholzite ($CaZn_2(PO_4)_2 \cdot 2(H_2O)$), smithsonite ($ZnCO_3$), willemite ($Zn_2SiO_4$) and zn-sulfate ($ZnSO_4$).

The XANES spectra of the randomly chosen hotspots were averaged, the edge energy calibrated and the spectrum normalised. Linear combination fitting (LCF) was applied using IFEFFIT software on the pre-processed XANES spectra of the hotspots (Newville 2001). For each selected hotspot, the combination with the lowest χ^2 was chosen as the most likely combination of compounds in that hotspot. The accuracy of

the fitting depends on how well the standards represent the data. A reduced χ^2 smaller than 1 indicated a reliable fit. Owing to the limited number of standards, the best fit composition may not give the true composition, although it can provide an indication of primary forms of the element of interest and describe the chemical differences among the selected hotspots in a spatially-resolved manner.

Subsequently, impregnated soil samples were chemically analysed with an Agilent 7500cs ICP MS. The regions of interest were ablated using a high performance New Wave Nd Yag 213 UV laser. An optical microscope was used to find pores in the impregnated samples with a thickness of approximately 0.5 cm and a length of 3 cm. The pores did not always obviously contain organic matter. With the laser, the samples were ablated across the micropores over a length of 2 mm. The laser ablated at a speed of 10 $\mu m\ s^{-1}$ and the spotsize was 30 μm. The sensitivity was 4.7 $mg\ l^{-1}$ for Ca; 280 $ng\ l^{-1}$ for Mn; 86 $\mu g\ l^{-1}$ for Fe; 1.9 $\mu g\ l^{-1}$ for Zn and 290 $ng\ l^{-1}$ for Cu. Measurements were qualitative and only gave a representation of the depletion or accumulation of elements along the micropore. For quantitative measurements, calibration is necessary. This could be done with homogeneous samples. However, this would have defeated the purpose of the study insofar as our objective was to characterise the heterogeneity of the elements in the immediate vicinity of micropores in which we were interested. Another reason why quantitative measures were not possible was that the depth to which the laser ablated, and hence the volume of soil nebulised, was not always constant (Weis *et al*. 2005).

RESULTS AND DISCUSSION

Of the few pores from the intact samples and the thin sections that were studied only one representative of each sample type was selected for consideration in this section of the paper. An intact sample containing a black decaying root was scanned over an area of 1 cm by 0.2 cm. The XRF images showed that Ca was concentrated in the channel containing the root (Figure 1). The pore selected contained organic matter from a decaying root and this may have been a source of the Ca, given that roots can accumulate Ca (Singh and Jacobson 1979). Another source may be Ca from the soil solution adsorbed onto the organic matter. Pores in the thin sections did not always contain decaying organic matter but pores selected always had coatings of organic matter (Figure 2). As shown on the distribution maps, Ca was also concentrated in the pores (Figure 3). In this case, Ca could have been adsorbed from the soil solution onto the pore surface. So it seems that either root activity concentrates Ca at pore walls and in pores solely by organic matter decay, or water extraction by roots can be also responsible for accumulation of Ca in and around pore walls. With the techniques used in the current study (synchrotron based hard x-ray absorptionspectroscopy) it was not possible to directly obtain chemical form(s) of Ca accumulated in and at the surface of pore walls. These soils were alkaline and pH generally increases with depth. Co-located elements (i.e., Cu) were mainly in carbonate forms and therefore, it is possible Ca accumulated, at least in part, as Ca carbonate. There is ample of evidence of Ca carbonate precipitation occurring in root biopores, and in the rhizosphere (Jaillard 1982; Callot et al. 1983; Hinsinger *et al*. 1998).

The correlation graphs originating from the XRF distribution maps showed that Mn and Zn were always strongly correlated with Fe in the intact samples and the thin sections (R^2 for Fe and Mn = 0.93, Figure 1 and R^2 for Fe and Mn = 0.92, Figure 3). The correlations of Mn and Fe were based on the low energy maps taken below the

absorption edge of Fe. Calcium and Cu were much less positively correlated to Fe than Mn and Zn. Calcium was mainly accumulated in pores whereas Fe, Mn, Cu and Zn were mainly accumulated in soil. Calcium, Mn, Zn and Cu were always more correlated with Fe in the intact samples than in the thin sections, a result that has its explanation in the difference in effective sampling depth of the two sample types. The pores selected were always those exposed on the surface of the samples. Fluorescence x-ray signals measured in these experiments could have escaped from a maximum sample depth of about 50 μm. Given that intact samples were approximately 10 mm thick spectral information will have been gathered, not only from the pore surface but also the soil matrix. Because the soil contains a total Fe concentration of approximately 4 %, a considerable contribution to the Fe spectral signatures will have come from the matrix. The thickness of the thin sections was only 20 μm; therefore, the influence of matrix Fe would have been less significant. Data from hotspots suggested that most of the Mn existed in reduced form (Table 1). More than 50 % of Mn occurred as Mn phosphate-like species (hureaulite and switzerite) and those species could also contained reduced Fe. In contrast, the Mn hotspots selected in the intact samples had a significant fraction of Mn as Mn (IV) oxides (birnessite and MnO_2) in addition to Mn phosphate-like species. This was not observed in the thin sections. It is, however, not certain whether this was an artefact of thin section preparation, beam-induced reduction of Mn in soil thin sections (i.e., due to interaction with resin) or due to the fact that larger soil volume was exposed in the intact sample XANES data collection. Furthermore, the measurements close to the pore surface did not differ from the ones further into the soil matrix (Figure 4). In most Sodosols only a small proportion of Fe is available for plants because of the oxidized form in which the Fe is present. The three chemical conditions and processes

primarily affecting Fe availability to plants are pH, redox status and chelation (McFarlane 1999). The distribution maps showed that there was no enrichment of Fe around the selected pores (Figure 1 and 3) but that it was distributed randomly throughout the areas chosen for analysis. The XANES spectra suggested that Fe was mostly present in oxidised form (Table 2). Oxide-like bindings such as those of goethite and hematite were found in the hotspots selected in the intact samples and the thin sections. Some spots in the intact samples appeared to contain greenrust-Cl-like and greenrust-sulfate-like bindings but these forms were not found in the thin sections. In contrast, magnetite was always found in the thin sections (except for one hotspot) but never in the intact samples. Greenrust ((Fe, $Mg^{2+})_6(Fe^{3+})_2(OH)_{18}.4(H_2O)_{18}$) and magnetite ($Fe_3O_4$) both are oxides with a mixture of oxidised and reduced Fe. The only conclusion that could be made was that in the selected hotspots, a mixture of oxidised and reduced Fe was present. The hotspots selected in the thin sections always had a higher proportion of mixed oxidation forms of Fe compared with hotspots selected on the intact samples. Therefore, it could not be concluded that the Fe speciation in the intact sample was different from the ones in the thin sections. The amount of standard used in this type of study is limited. Given that soil is highly heterogeneous we could not state that the bindings in the hotspots were exactly the same as the bindings of the standards. We concluded that, in all these hotspots, Fe-O-like minerals were present and that these were a mixture of Fe in II and III oxidation state similar to the ones found in the standards (Figure 5). In only one hotspot in the thin section was Fe found in a phosphate binding (vivianite). Zinc sometimes accumulated around the micropores but was also present in higher concentrations away from the pore (Figures 1 and 3). Linear combination fitting of the XANES and EXAFS region of the absorption spectra showed that the speciation of Zn

for the hotspot at the edge of the pore and further in the soil matrix chosen in the intact samples were very similar and in forms resembling hydrozincite, Zn-sulfate and willemite. The same was found for the hotspots selected on the thin sections: zinc was always found associated with sulfates at the pore surface. Franklenite-like forms were found at the pore edge whereas Zn adsorbed on ferrihydrite was found in the soil matrix. Only one instance of smithsonite-like bindings was found and this at the pore surface. This could be due to the higher CO_2 levels inside soil pores that favour the formation of carbonates. The one occurrence of scholzite was in the soil matrix.

Copper was only present in small amounts in the soil (< 10 ppm in the whole soil profile). The XRF maps of the thin sections showed that Cu was enriched at the edges of the areas where Ca was located or in the same areas (Figure 3). These areas of enrichment were coincident with organic matter coatings. Previous studies have found that Cu is associated with organic matter (Jacobson *et al*. 2007). In this study, only two hotspots in the area close to the pore in the thin sections could be analysed because of the low concentration of Cu in the soil. The components resulting from the linear combination fitting were different for both hotspots. However, both were composed of approximately 70 % carbonate and 30 % phosphate (Table 4). Again, this could be due to higher levels of CO_2 in and in the vicinity of soil pores, favouring the formation of carbonates.

The distribution of elements of interest across a section of a micropore in impregnated samples were measured by LA-ICP-MS and compared with XANES and EXAFS data of the same section. Measurements from 0 s to 10 s at the beginning of the X-axis could not be accounted for as the instrument always needed a period to adjust (Figures 7 and 8). By viewing the ablating point on the sample on the screen of the microscope and comparing it with the counts of the elements detected, it was

established that the decrease in counts of silicon (Si) was a sensitive measure of the location of the micropore. Because we can expect Si distribution abundantly all throughout soil but low or closer-to-background concentrations wherever we have pores. The point with the lowest counts was the middle of the pore and this can be attributed to pore geometry viz. approximate cylindrical shape of pores. Although in all of the μ-XRF maps indicated Ca was concentrated in the micropores Ca was detected only in some pores by the LA-ICP-MS. The graphs however, show that wherever there was an accumulation of Ca, there was also an accumulation of Fe and Mn (Figure 7 see ~ 20 s, Figure 8 see ~10 to 50 s). This is in contradiction with the distribution maps by μ-XRF. The differences are probably a result of the different volumes of soil material sampled during measurement; sampling depth (effective fluorescence signal depth) for μ-XRF was 50 μm whereas that for LA-ICP-MS was greater. Because Fe is relatively depleted at the very surface of the micropore, LA-ICP-MS will detect a greater proportion of Fe than μ-XRF. There were accumulations of Mn, Zn and Cu in proximity of the micropore. It should be noted here that care has to be taken when interpreting results obtained by LA-ICP-MS. Elemental fractionation depends on characteristics of the sample such as optical absorption behaviour. In a heterogeneous medium such as soil, this will vary between samples and therefore, overcoming this problem for matrixindependent quantification becomes a problem (Weis *et al*. 2005). The high degree of heterogeneity of the elements in the samples and their inhomogeneous distribution makes it impossible to have precise and accurate results that allow quantification (Jimenez *et al*. 2007).

Every pore created by roots and used by subsequent roots has a different history. The inhomogeneity in elemental concentration and spatial distribution will be greater at smaller scale than at larger scale. Rhizosphere chemistry will depend on the type of

root (e.g. root hair, mature root), state of decomposition, extent and diversity of occupancy of pore, and types of plants. Further complexity arises from transport of particles in suspension and solutions, a process dependent on a range of factors such as pore size and pore continuity. Surface analytical techniques such as those employed here have a significant role to play in refining our understanding of nutrient form, concentration and availability and how plant roots affect these in space and time.

In this investigation we attempted to study microstructure, in as undisturbed condition as possible, by using intact soil aggregates and thin sections prepared following vacuum impregnation with resin. However, many surface-sensitive techniques require a flat surface. Intact samples cannot be polished, and when surfaces are flattened, smearing occurs which alters the organisation of soil particles that could lead to problems when the chemistry of the surface is studied. Soils of low coherence fragment readily. We attempted to study the chemical nature of the rhizosphere across the E horizon-B horizon boundary but the samples fragmented and our study was confined to the upper B horizon.

CONCLUSION

This study shows that one pore can be drastically different from another. However, there was no difference in chemistry of these elements at the pore surface and <500 μm (Jassogne et al. 2009) to 10,000 μm from it (current study). As observed for micropores in our 2009 study, it appeared that the influence of the micropore was to concentrate Zn, Mn, Cu within and in the immediate vicinity of it but that there was no significant influence of the micropore on the chemical form of these elements. The chemical form of these 3 elements was similar at the pore surface and in the matrix. A

larger area around the micropore may need to be studied to see whether the influence on the chemical form of these elements varies at a larger scale (> 1 cm).

The difference in micro-spatial chemistry between the thin sections and the intact samples can be attributed to the thickness of the sample analysed. This resulted in Mn, Zn and Cu having stronger correlations with Fe in the thin sections compared with the intact samples suggesting that thinness of samples is important to define "real" elemental relationships. Differences observed between μ-XRF and LC-ICP-MS can be mainly attributed to lower detection limit of LA-ICP-MS compared to synchrotron based μ-XRF and the differences in effective sampling depths by these techniques. The combination of these non-invasive techniques, especially synchrotron based x-ray techniques, has given more insights in root/soil interactions.

REFERENCES

Adcock D, McNeill AM, McDonald GK, Armstrong RD (2007) Subsoil constraints to crop production on neutral and alkaline soils in south-eastern Australia: a review of current knowledge and management strategies. *Australian Journal of Experimental Agriculture* **47**, 1245-1261.

Bouma J (1992) Influences of soil macroporosity on environmental quality. In 'Advances in Agronomy'. (Ed. DL Sparks) (Academic Press: New York)

Callot G, Chamayou H, Maertens C, Salsac L (1983) Mieux comprendre les interactions sol-racine. Incidence sur la nutrition minérale. INRA, Paris, p 326

Chittleborough DJ (1992) Formation and pedology of duplex soils. *Australian Journal of Experimental Agriculture* **32**, 15-25.

Eldridge DJ, Freudenberger D (2005) Ecosystem wicks: Woodland trees enhance water infiltration in a fragmented agricultural landscape in eastern Australia. *Australian Journal of Ecology* **30**, 336-347.

Hinsinger P (1998) How do plant roots acquire mineral nutrients? Chemical processes involved in the rhizosphere. Adv Agron 64:225–265

Hinsinger P, Plassard C, Jaillard B (2006) Rhizosphere: A new frontier for soil biogeochemistry. *Journal of Geochemical Exploration* **88**, 210-213.

Isaure MP, Manceau A, Geoffroy N, Laboudigue A, Tamura N, Marcus MA (2005) Zinc mobility and speciation in soil covered by contaminated dredged sediment using micrometer-scale and bulk-averaging X-ray fluorescence, absorption and diffraction techniques. *Geochimica et Cosmochimica Acta* **69**, 1173-1198.

Isbell RF (1996) 'The Australian Soil Classification'. (CSIRO publishing: Melbourne)

Jacobson AR, Dousset S, Andreux F, Baveye PC (2007) Electron microprobe and synchrotron X-ray fluorescence mapping of the heterogeneous distribution of copper in high-copper vineyard soils. *Environmental Science and Technology* **41**, 6343-6349.

Jaillard B (1982) Relation entre dynamique de l'eau et organisation morphologique d'un sol calcaire. Science du Sol 20:31–52.

Jaillard B (1987b) Techniques for studying the ionic environment at the soil-root interface. In: Methodology in soil-K research (I.P.I. Ed.). International Potassium Institute, Bâle, pp 231-245.

Jassogne L, Hettiarachchi G, Chittleborough D, McNeill A (2009) Distribution and speciation nutrient elements around micropores. *Soil Science Society of America Journal* **73**, 1319-1326.

Jimenez, MS, Gomez MT, Castillo JR (2007) Multi-element analysis of compost by laser ablation-inductively coupled plasma mass spectrometry. *Talanta* **72**, 1141-1148.

Manceau A, Marcus MA, Tamura N, Proux O, Geoffroy N, Lanson B (2004) Natural speciation of Zn at the micrometer scale in a clayey soil using X-ray fluorescence, absorption, and diffraction. *Geochimica et Cosmochimica Acta* **68**, 2467-2483.

McCully M (2005) The rhizosphere: the key functional unit in plant/soil/microbial interactions in the field. implications for the understanding of allelopathic effects. In 'Proceedings of the 4th World Congress on Allelopathy, "Establishing the Scientific Base"'. (Eds J Harper, M An, H Wu, J Kent) (Centre for Rural Social Research, Charles Sturt University, Waga Waga)

McCully ME (1999) Roots in soil: unearthing the complexities of roots and their rhizospheres. *Annual Review of Plant Physiology and Plant Molecular Biology* **50**, 695-718.

McFarlane JD (1999) Iron. In 'Soil analysis: an interpretation manual' . (Eds KI Peverill, LA Sparrow and DJ Reuter) (CSIRO publishing: Collingwood, Australia)

Newville M (2001) IFEFFIT: interactive XAFS analysis and FEFF fitting. *Journal of Synchrotron Radiation* **8**, 322-324.

Pankhurst CE, Pierret A, Hawke B, Kirby JM (2002) Microbiological and chemical properties of soil associated with macropores at different depths in a red-duplex soil in NSW Australia. *Plant and Soil* **238**,11-20.

Pierret A, Moran CJ, Pankhurst CE (1999) Differentiation of soil properties related to the spatial association of wheat roots and soil macropores. *Plant and Soil* **211,** 51-58.

Singh C, Jacobson L (1979) The accumulation and transport of calcium in Barley roots. *Physiologia Plantarum* **45**, 443-447.

Soil Survey Staff (1999) Soil Taxonomy. In 'Agriculture Handbook 436'. (Ed. Natural Resources Conservation Service) (USDA: Washington, DC)

Stewart JB, Moran CJ, Wood JT (1999) Macropore sheath: quantification of plant root and soil macropore association. *Plant and Soil* **211**, 59-67.

Strawn D, Doner H, Zavarin M, McHugo S (2002). Microscale investigation into the geochemistry of arsenic, selenium, and iron in soil developed in pyritic shale materials. *Geoderma* **108**, 237-257.

Vannoordwijk M, Kooistra MJ, Boone FR, Veen BW, Schoonderbeek D (1992) Root-Soil Contact of Maize, as Measured by a Thin-Section Technique .1. Validity of the Method. *Plant and Soil* **139**, 109-118.

Voegelin A, Weber FA, Kretzschmar R (2007) Distribution and speciation of arsenic around roots in a contaminated riparian floodplain soil: Micro-XRF element mapping and EXAFS spectroscopy. *Geochimica et Cosmochimica Acta* **71**, 5804-5820.

Weis P, Beck HP, Gunther D (2005) Characterizing ablation and aerosol generation during elemental fractionation on absorption modified lithium tetraborate glasses using LA-ICP-MS. *Analytical and Bioanalytical Chemistry* **381**:212-224.

Yunusa IAM, Mele PM, Rab MA, Schefe CR, Beverly CR (2002) Priming of soil structural and hydrological properties by native woody species, annual crops, and a permanent pasture. *Australian Journal of Soil Research* **40**, 207-219.

Figure captions

Figure 1: Distribution maps of Ca, Mn, Fe, Zn and Cu around a pore obtained by μ-XRF in an intact sample and the correlation between these elements.

Figure 2: Optical photomicrograph of the pore scanned by μ-XRF on the thin section represented in Figure 3.

Figure 3: Distribution maps of Ca, Mn, Fe, Zn and Cu around a pore by μ-XRF in a thin section and the correlation of these elements.

Figure 4: Some spectra and respective linear combination fittings of hotspots of Mn selected in the immediate vicinity of the pore (close) and in the soil matrix > 5 mm from the pore surface in the intact samples and > 1mm from the pore surface in the thin sections (far).

Figure 5: Some spectra and respective linear combination fittings of hotspots of Fe selected in the immediate vicinity of the pore (close) and in the soil matrix > 5 mm

from the pore surface in the intact samples and > 1mm from the pore surface in the thin sections (far).

Figure 6: Some spectra and respective linear combination fittings of hotspots of Zn selected in the immediate vicinity of the pore (close) and in the soil matrix > 5 mm from the pore surface in the intact samples and > 1mm from the pore surface in the thin sections (far).

Figure 7: Relative distribution of Si, Ca, Mn, Fe, Cu and Zn across micropore-1 using LA-ICP-MS. Ca is enriched in the pore.

Figure 8: Relative distribution of Si, Ca, Mn, Fe, Cu and Zn along a line across micropore-2 using LA-ICP-MS. Ca is impoverished in the pore.

Tables

Table 1: Fractions of Mn species in selected 'Mn-hotspots' in the area close and far from the soil micropore in an intact soil sample and in a thin section.

		birnessite	hureaulite	switzrite	Mn_2O_3	MnO_2	red-$\chi^{2\dagger}$
close	1	0.00	0.00	0.76	0.24	0.00	0.011
far	2	0.11	0.66	0.25	0.00	0.00	0.018
	3	0.056	0.00	0.58	0.00	0.36	<0.010
close_ts ††	4	0.00	0.36	0.64	0.00	0.00	<0.010

$^{\dagger}\chi^2 = \Sigma\,[(\text{fit} - \text{data})/\varepsilon]^2 / (N_{data} - N_{components})$ is the chi-square statistic. Here ε is the estimated uncertainty in the normalized XANES data (taken as 0.01 for all data). The sum is over N_{data} points and $N_{components}$ is the number of components in the fit. The total percentage was constrained to be 100% in all fits. Typical uncertainties in the fractions listed for each standard component are 5%.

††ts: thin section

Table 2: Fractions of Fe species in selected 'Fe-hotspots' in the area close and far from the soil micropore in an intact soil sample and in a thin section

		Fe_2O_3	goethite	greenrust-Cl	greenrust-S	Fe_3O_4	vivianite	red–$\chi^{2\dagger}$
close								
	1	0.64	0.12	0.069	0.17	0.00	0.00	<0.010
	2	0.49	0.51	0.00	0.00	0.00	0.00	<0.010
	3	0.69	0.31	0.00	0.00	0.00	0.00	<0.010
far								
	4	0.58	0.42	0.00	0.00	0.00	0.00	<0.010
	5	0.72	0.23	0.054	0.00	0.00	0.00	<0.010
	6	0.05	0.95	0.00	0.00	0.00	0.00	<0.010
close_ts ††								
	7	0.69	0.00	0.00	0.00	0.13	0.18	<0.010
	8	0.59	0.41	0.00	0.00	0.00	0.00	<0.010
	9	0.24	0.52	0.00	0.00	0.23	0.00	<0.010
	10	0.26	0.56	0.00	0.00	0.18	0.00	<0.010
	11	0.00	0.77	0.00	0.00	0.23	0.00	<0.010
far_ts								
	12	0.18	0.61	0.00	0.00	0.21	0.00	<0.010
	13	0.34	0.55	0.00	0.00	0.11	0.00	<0.010

$^{\dagger}\chi^2 = \Sigma\,[(\text{fit} - \text{data})/\varepsilon]^2 / (N_{data} - N_{components})$ is the chi-square statistic. Here ε is the estimated uncertainty in the normalized XANES data (taken as 0.01 for all data). The sum is over N_{data} points and $N_{components}$ is the number of components in the fit. The total percentage was constrained to be 100% in all fits. Typical uncertainties in the fractions listed for each standard component are 5%.

††ts: thin section

Table 3: Fractions of Zn species in selected 'Zn-hotspots' in the area close and far from the soil micropore in an intact soil sample and in a thin section.

		franklenite	hydrozincite	zn-sulfate	ferrihydrite adsorbed zn	willemite	smithsonite	scholzite	red-$\chi^{2\dagger}$
close									
	1	0.00	0.66	0.00	0.00	0.34	0.00	0.00	0.035
	2	0.00	0.23	0.00	0.00	0.00	0.77	0.00	0.15
far									
	3	0.00	0.18	0.60	0.00	0.23	0.00	0.00	0.013
close_ts ††									
	4	0.00	0.49	0.12	0.00	0.39	0.00	0.00	0.00
	5	0.00	0.34	0.22	0.00	0.44	0.00	0.00	0.00
	6	0.29	0.39	0.17	0.15	0.00	0.00	0.00	0.00
	7	0.00	0.00	0.38	0.10	0.52	0.00	0.00	0.00
	8	0.29	0.00	0.40	0.00	0.00	0.31	0.00	0.00
far_ts									
	9	0.00	0.00	0.51	0.087	0.40	0.00	0.00	0.00
	10	0.00	0.49	0.00	0.00	0.16	0.00	0.35	0.016
	11	0.00	0.00	0.00	0.30	0.70	0.00	0.00	0.064

† $\chi^2 = \Sigma\,[(\text{fit} - \text{data})/\varepsilon]^2 / (N_{data} - N_{components})$ is the chi-square statistic. Here ε is the estimated uncertainty in the normalized XANES data (taken as 0.01 for all data). The sum is over N_{data} points and $N_{components}$ is the number of components in the fit. The total percentage was constrained to be 100% in all fits. Typical uncertainties in the fractions listed for each standard component are 5%.

†† ts: thin section

Table 4: Fractions of Cu species in selected 'Cu-hotspots' in the area close to the soil micropore in a thin section (ts).

		malachite	nissonite	azurite	calcosiderite	red-χ^2
close_ts						
	1	0.69	0.31	0.00	0.00	19.55
	2	0.00	0.00	0.70	0.30	121.63

$^{\dagger}\chi^2 = \Sigma\,[(\text{fit} - \text{data})/\varepsilon]^2 / (N_{data} - N_{components})$ is the chi-square statistic. Here ε is the estimated uncertainty in the normalized XANES data (taken as 0.01 for all data). The sum is over N_{data} points and $N_{components}$ is the number of components in the fit. The total fractions was constrained to be 100% in all fits. Typical uncertainties in the fractions listed for each standard component are 5%.

Figure 1

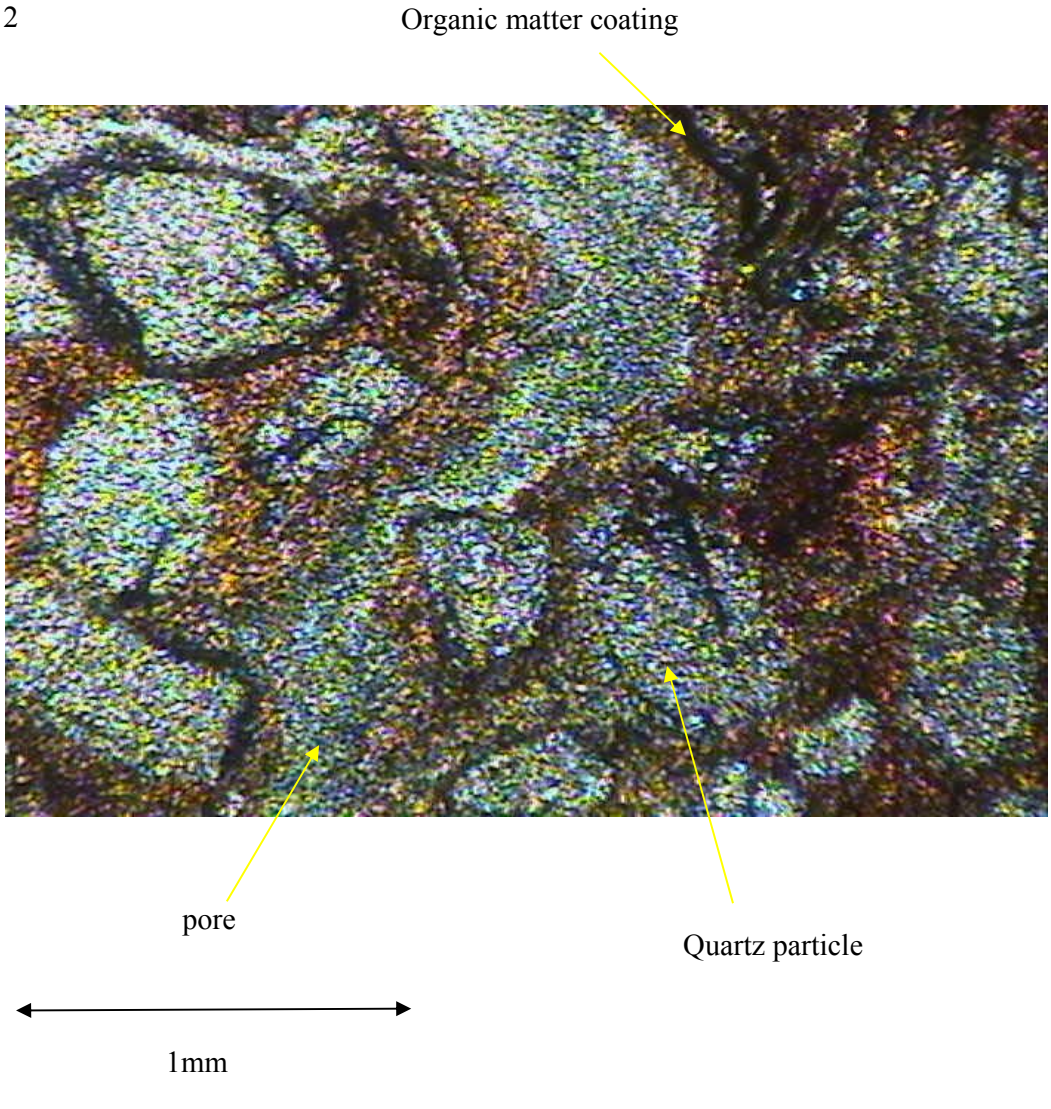

1 **Figure 2**

2

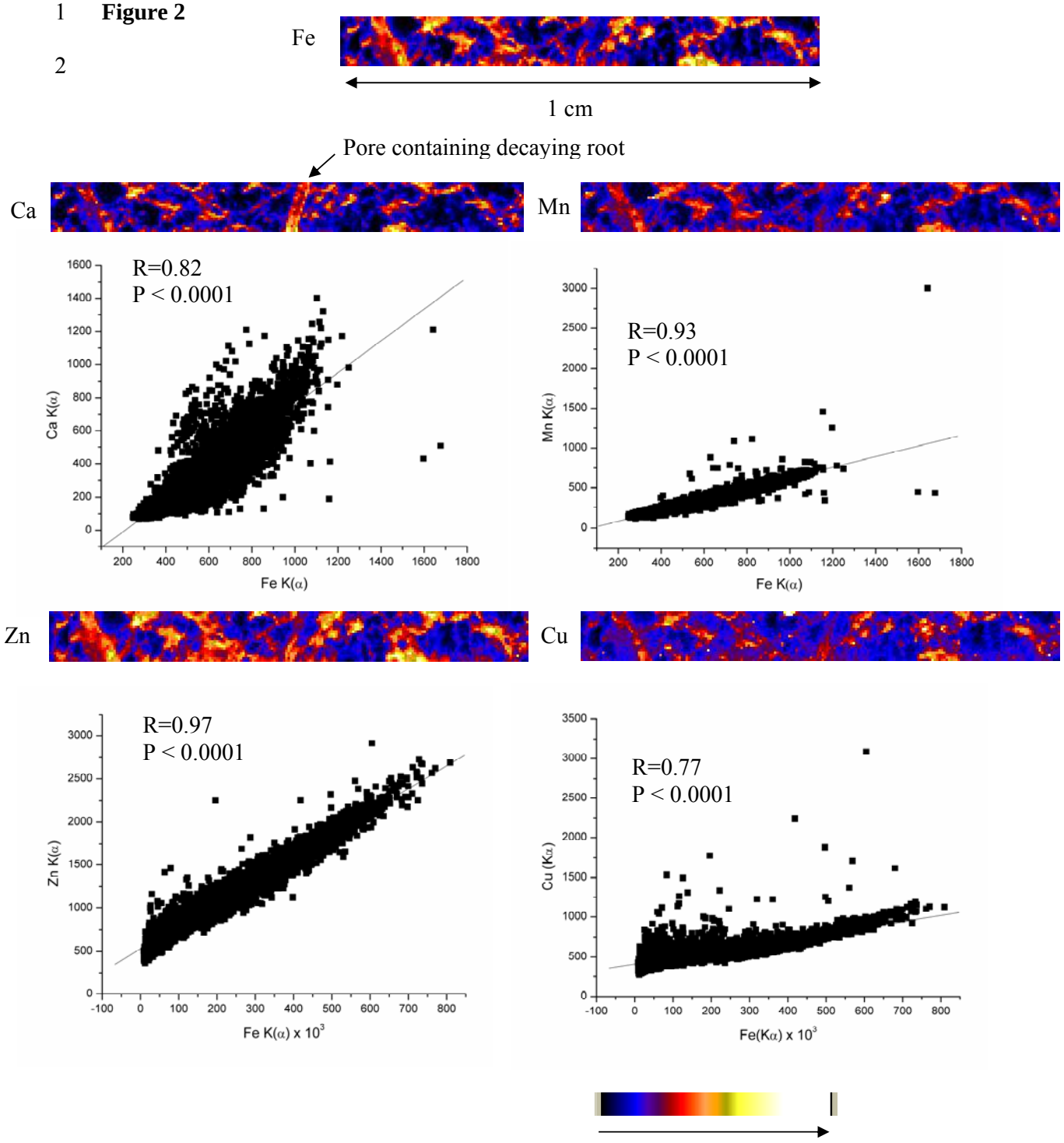
Fe
1 cm
Pore containing decaying root
Ca
Mn
R=0.82
P < 0.0001
Ca K(α)
Fe K(α)
R=0.93
P < 0.0001
Mn K(α)
Fe K(α)
Zn
Cu
R=0.97
P < 0.0001
Zn K(α)
Fe K(α) x 10³
R=0.77
P < 0.0001
Cu (Kα)
Fe(Kα) x 10³

Figure 3
Repeat colour scale as for Figure 2

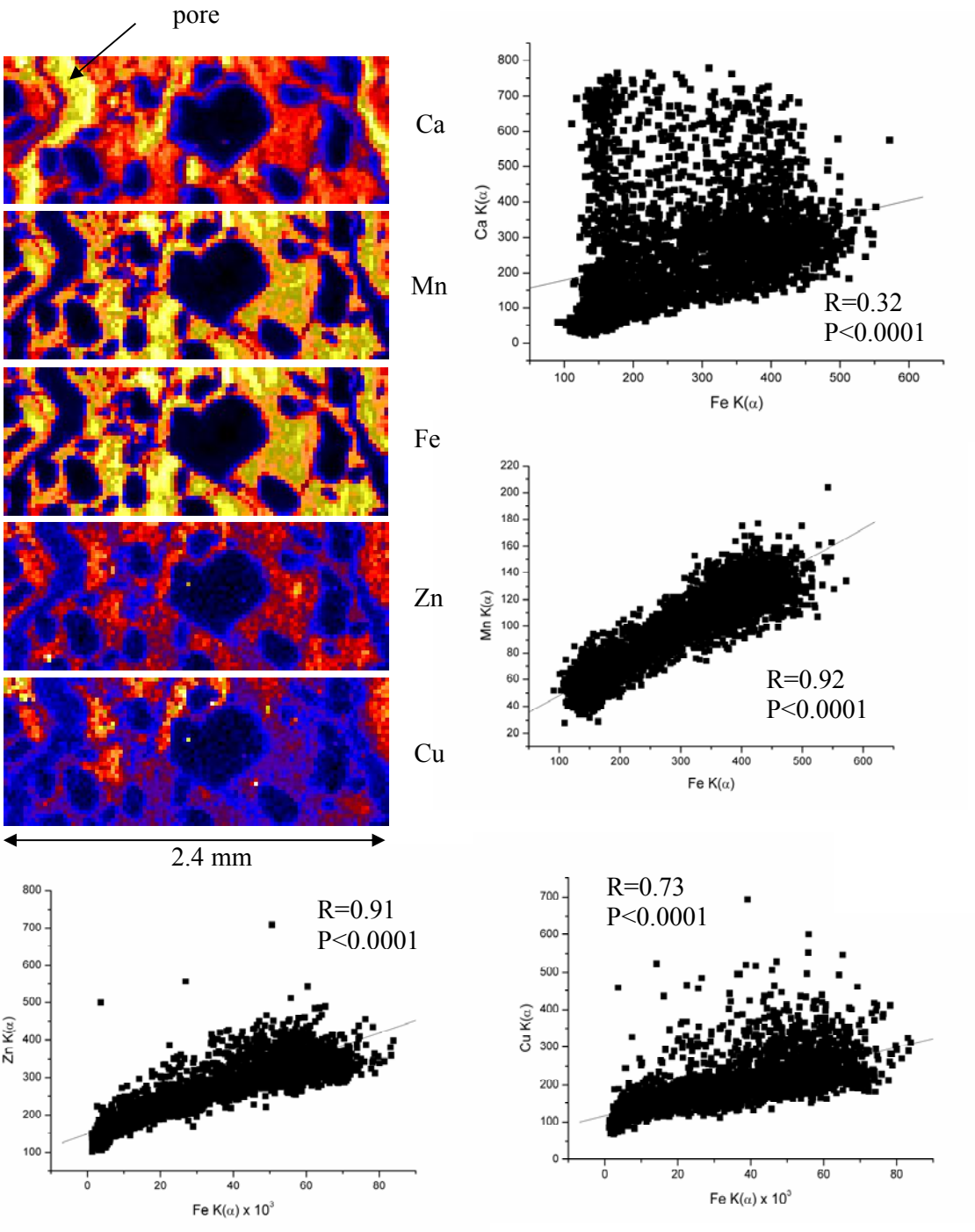

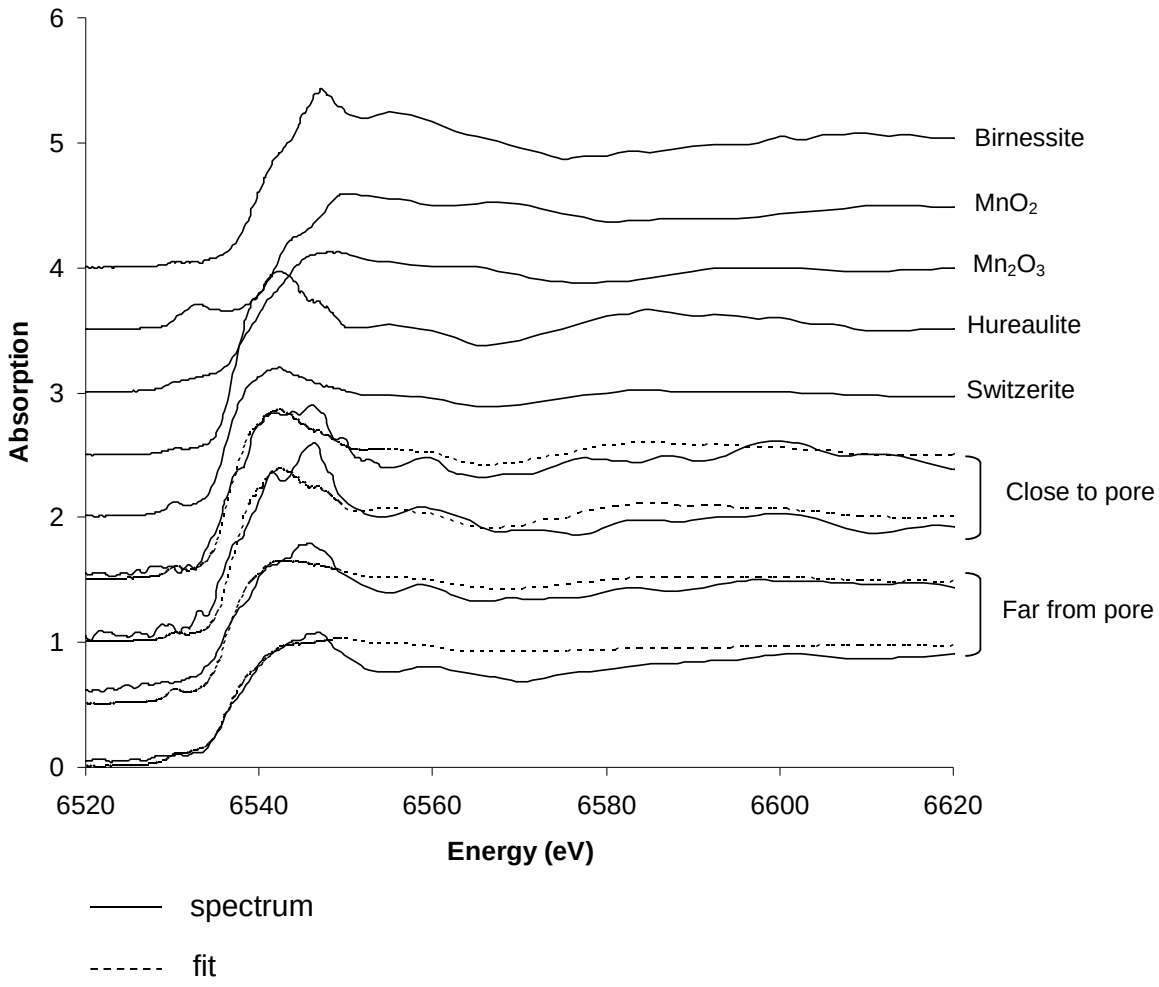
Absorption
Energy (eV)
6520
6540
6560
6580
6600
6620
0
1
2
3
4
5
6
Birnessite
MnO2
Mn2O3
Hureaulite
Switzerite
Close to pore
Far from pore
spectrum
fit

Figure 4

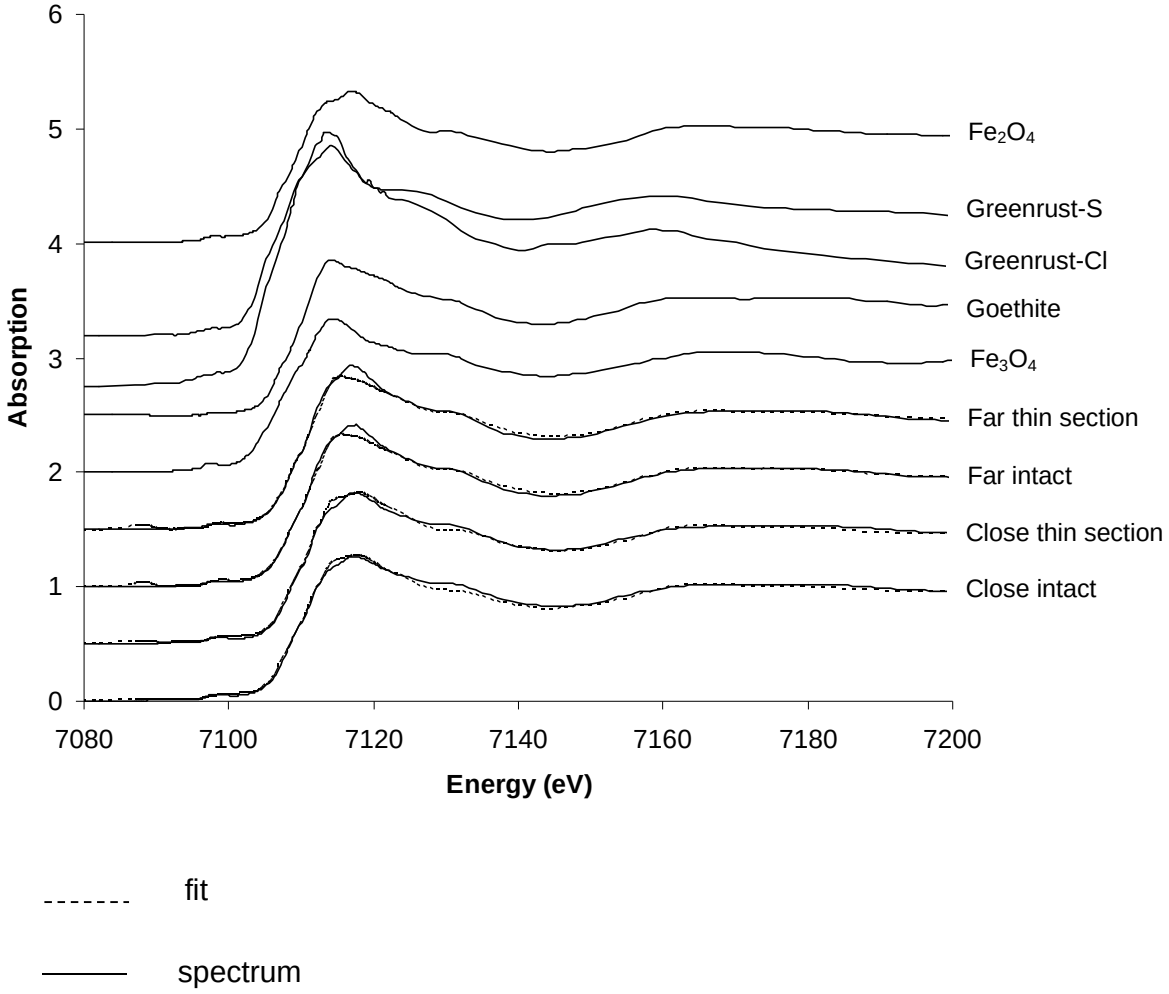
Absorption
Energy (eV)
7080
7100
7120
7140
7160
7180
7200
0
1
2
3
4
5
6
Fe_2O_4
Greenrust-S
Greenrust-Cl
Goethite
Fe_3O_4
Far thin section
Far intact
Close thin section
Close intact
fit
spectrum

Figure 5

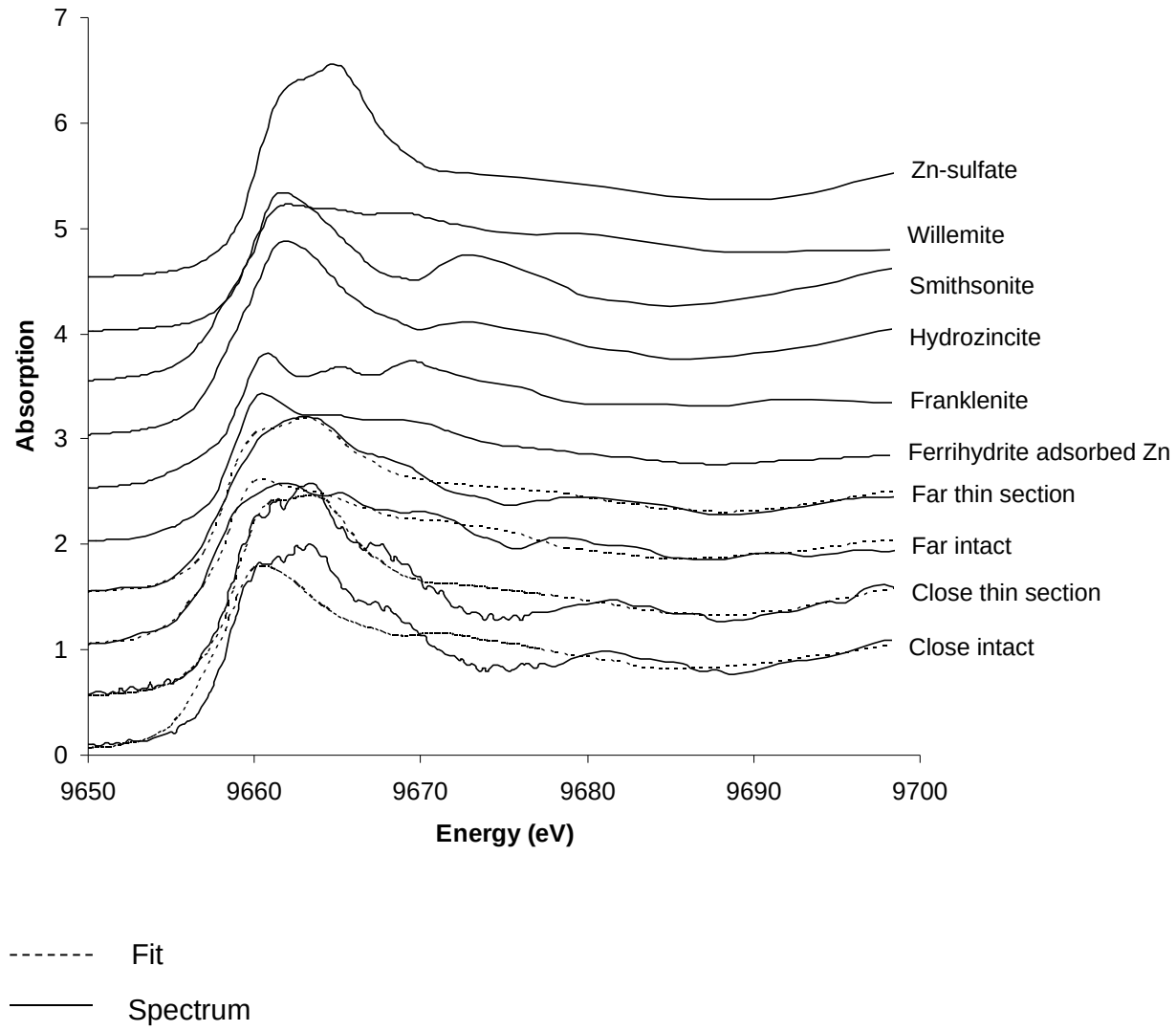
Absorption
Energy (eV)
9650
9660
9670
9680
9690
9700
0
1
2
3
4
5
6
7
Zn-sulfate
Willemite
Smithsonite
Hydrozincite
Franklenite
Ferrihydrite adsorbed Zn
Far thin section
Far intact
Close thin section
Close intact
Fit
Spectrum

Figure 6

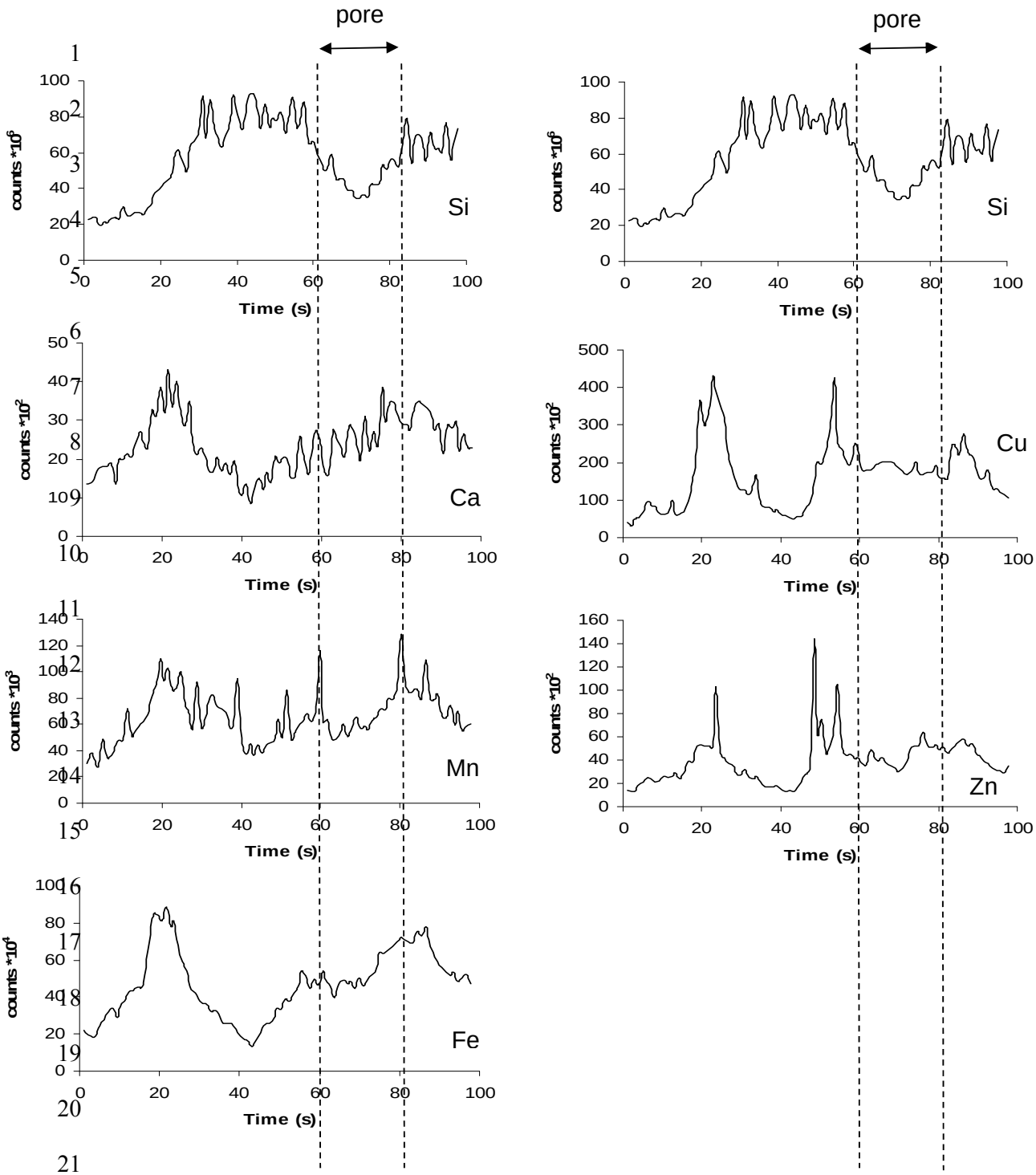
pore
counts *10^6
Si
Time (s)
counts *10^2
Ca
Time (s)
counts *10^3
Mn
Time (s)
counts *10^4
Fe
Time (s)
pore
counts *10^6
Si
Time (s)
counts *10^2
Cu
Time (s)
counts *10^2
Zn
Time (s)

Figure 7

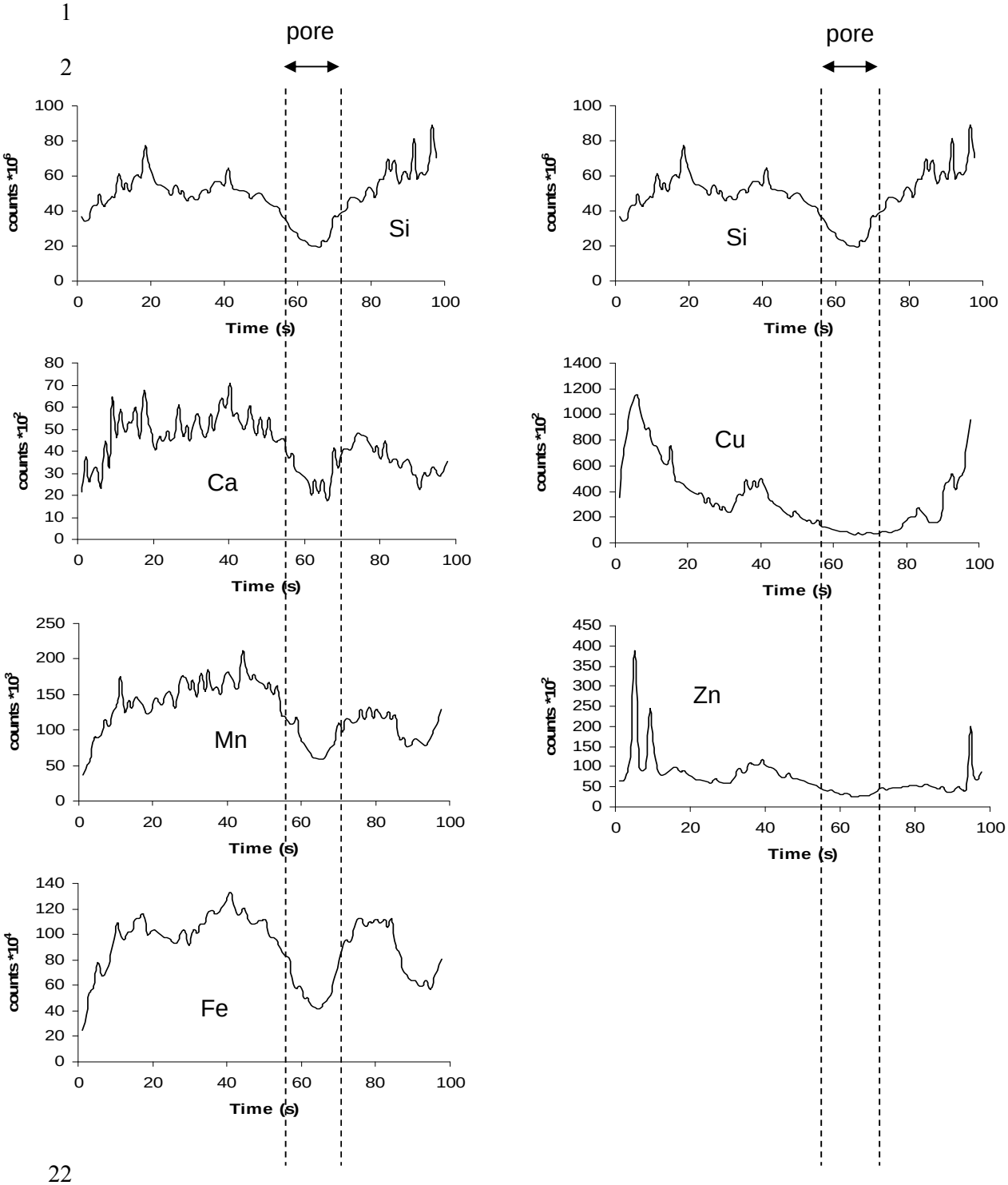
pore
pore
counts *10^6
Si
Time (s)
counts *10^2
Ca
Cu
counts *10^3
Mn
counts *10^2
Zn
counts *10^4
Fe

Figure 8